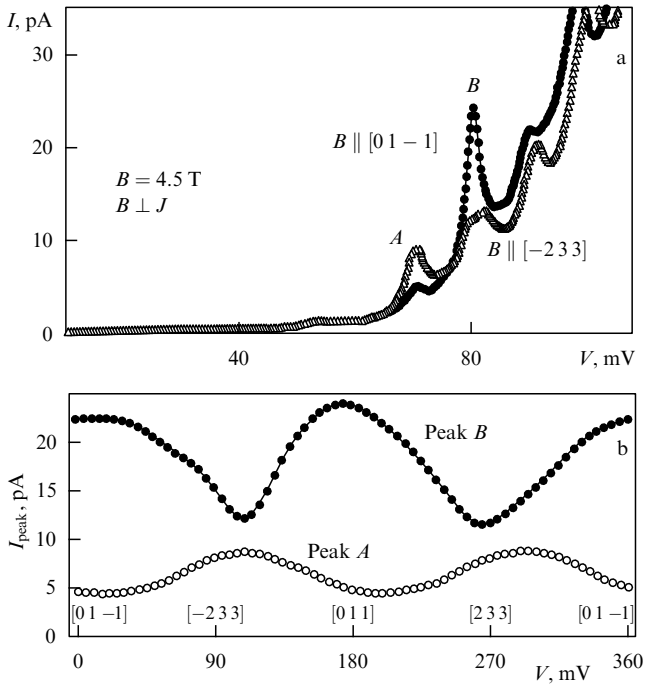

Figure 3. (a) Current–voltage characteristics $I(V)$ for the case of a magnetic field $B = 4.5$ T that is perpendicular to the electric current. The first curve (small black disks) represents the case where $B||[-1\ -1]$, and the second curve (small open triangles) represents the case where $B||[-233]$. (b) Angular dependence of the peak currents for the resonances A and B.

(emitter) and final (quantum dot) states between which the tunnel transition occurs [5, 6]. Note that the initial states of the emitter are rather weakly localized in the real space, in contrast to the strongly localized states of quantum dots. Hence $\Phi_i(k)$ in the k-space is represented by a Dirac delta function, which is nonzero only in the vicinity of $k = 0$. And since the tunnel current is determined by the square of the matrix element which contains both $\Phi_i(k)$ and $\Phi_f(k)$, the fact that $\Phi_i(k)$ is a Dirac delta function makes it possible to determine the shape of the function

$$\Phi_f(k) = \Phi_{QD}(k)\,,$$

by varying B and hence k. Thus, in reality, by measuring the dependence $I(B)$ [or $G(B)$] for a certain direction of B, we can find the shape of $|\Phi_{QD}(k)|^2$ along the direction of k perpendicular to B. Then, rotating B in the (X, Y) plane and measuring $I(B)$ (in a sequence) for different orientations of B, we obtain the complete spatial profile of $|\Phi_{QD}(k_x, k_y)|^2$, which is the projection of the probability density of a given electronic state of the quantum dot in the k-space in the plane perpendicular to the current [3].

Figure 4 depicts the profiles of differential conductance

$$G(B) = \frac{dI}{dV} \sim \left|\Phi_{QD}(k_x, k_y)\right|^2$$

in the (k_x, k_y) plane for the two quantum-dot states corresponding to Figs 3a, b. The resulting contour maps visualize the probability density distribution of the wave functions of the ground and excited states of a quantum dot. The electron wave functions are biaxially symmetric in the growth plane with the axes corresponding (to within measurement errors of about 15°) to the principal crystallographic

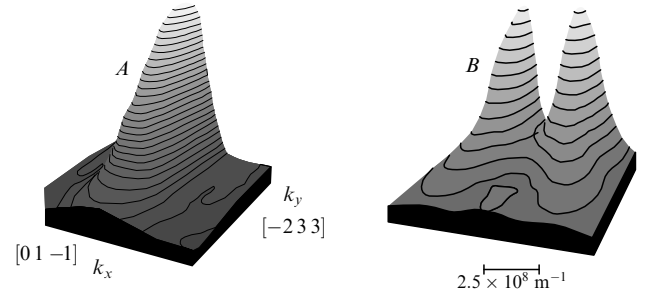

Figure 4. Profiles of the differential conductance, $G(B) = dI/dV \sim |\Phi_{QD}(k_x, k_y)|^2$, in the ($k_x$, k_y) plane for the two states of the quantum dots, corresponding to Figs 3a, b. The contour maps visualize the probability density distribution of the wave functions of the ground and excited states of a quantum dot.

directions X and Y for a (311) substrate orientation. For a (100) substrate we also obtained the characteristic images of the probability density for the ground and excited SAQD states.

The main result of the present work is a method that makes it possible to extract experimental information about the probability density distribution of the wave functions of electrons in self-assembled quantum dots. So far the proposed method is the only nondestructive technique for creating maps of the wave functions in SAQDs and has been applied to the given class of problems for the first time.

This work was made possible by grants from the Russian Foundation for Basic Research (grants 00-02-17903 and 01-02-17844), the Physics of Solid Nanostructures Program (97-1057), INTAS–RFBR (2000-774), and EPSRC (UK). The authors are grateful to V A Tulin and V G Lysenko for fruitful discussions and interest in the work, and to V V Belov and A Orlov for helping with the experiments.

References

1. Bimberg D, Grundmann M, Ledentsov N N *Quantum Dot Heterostructures* (New York: John Wiley, 1999)
2. Topinka M A et al. *Science* **289** 2323 (2000)
3. Vdovin E E et al. *Science* **290** 122 (2000)
4. Hayden R K et al. *Phys. Rev. Lett.* **66** 1749 (1991)
5. Beton P H et al. *Phys. Rev. Lett.* **75** 1996 (1995)
6. Sakai J-W et al. *Phys. Rev. B* **48** 5664 (1993)

PACS numbers: 71.45.Gm , 71.55.Eq , 73.20.Mf , 73.40.Gk

DOI: 10.1070/PU2001v044n12ABEH001056

Tunneling spectroscopy of quasi-two-dimensional plasmons

V A Volkov, É Takhtamirov, D Yu Ivanov, Yu V Dubrovskiĭ, L Eaves, P C Main, M Henini, D K Maude, J-C Portal, J C Maan, G Hill

1. Introduction

In two-dimensional (2D) electron systems based on semiconductors with an isotropic, parabolic dispersion law, the electron motion along the interface and transverse to the interface separates. Hence, in a magnetic field B that is

perpendicular to the interface, the one-particle Landau levels (LL) from different subbands do not interact with each other, and crossing of these levels is possible [1]. The situation is quite different with 2D systems based on semiconductors with a highly nonparabolic spectrum, such as the narrow-gap semiconductor PbTe [2]. Tunnel measurements in the latter case demonstrate anticrossing of Landau levels belonging to different 2D subbands.

We were the first to discover the strong interaction between such Landau levels in a tunnel 2D system based on GaAs, which is a semiconductor with an almost perfect parabolic dispersion law for the electrons. Highly disordered samples were used in the experiments, which made it possible to resolve the tunnel transitions between two 2D systems with and without a change of the LL number in the $2D \rightarrow 2D$ tunneling process.

2. Measurements

2.1 Samples

We used a single-barrier $GaAs/Al_{0.4}Ga_{0.6}As/GaAs$ heterostructure with a barrier 12-nm thick and vertical tunnel transport. The barrier was separated from the highly doped junction regions by undoped spacers 50-nm thick. To form the 2D electron layers, we employed delta-doping with silicon with a concentration in each layer amounting to 3×10^{11} cm^{-2} at a distance of 5 nm on each side of the barrier. Wet etching was used to form mesoscopic structures 100 – 400 μm in diameter. The penetrability of the tunnel barrier was much lower than that of the spacer, whereby almost the entire voltage applied to the structure falls on the tunnel barrier. Measurements of Shubnikov – de Haas type oscillations of the tunnel current yielded a value of electron concentration in the 2D layers approximately equal to the value of the concentration of the doping impurity. A schematic of the band diagram for the structure under investigation is depicted in Fig. 1 for a zero bias voltage. A typical value of the electron mobility amounted to $\mu = 1000$ cm^2 V^{-1} s^{-1} at 4.2 K.

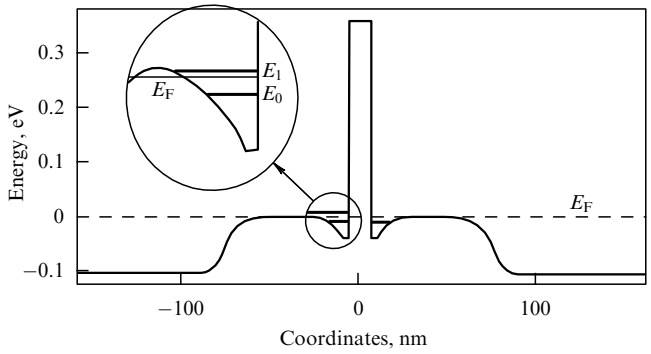

Figure 1. Schematic band diagram for a zero bias voltage. The inset shows the energy levels in 2D systems in greater detail: E_0 and E_1 are the bottoms of the ground and first excited 2D subbands, and E_F is the Fermi energy.

2.2 Experiment

Figure 2 depicts the differential tunneling conductivity G at 4.2 K (measured by the standard lock-in method) as a function of the applied bias voltage V_b in different magnetic fields up to 15 T. In a zero magnetic field (the lower curve in Fig. 2), the differential conductivity has a peak at zero bias voltage and two prominent 'arms' at higher bias voltages for both polarities of the applied voltage. The peak at zero bias voltage reflects the resonance nature of the tunneling between the ground states of the right and left electron systems, while the 'arms' appear because of resonance tunneling between the ground 2D subband ($n = 0$) of the emitter system and the first excited subband ($n = 1$) of the collector system. The very fact that there is a prominent peak in zero magnetic field and at zero bias voltage indicates that the fraction of tunneling processes proceeding with the conservation of momentum along the interface is relatively large, despite the large number of scattering centers. The development of these singularities as the magnetic field strength grows is due to tunneling between different Landau levels.

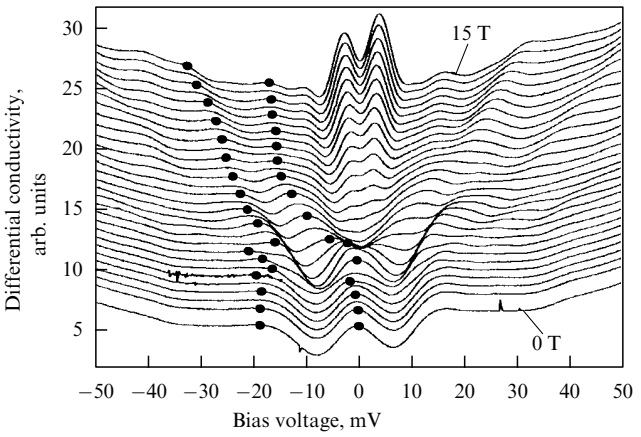

Figure 2. Differential tunneling conductivity at 4.2 K as a function of the bias voltage applied to the structure for a mesoscopic structure 400 μm in diameter. The lower curve corresponds to the case where $B = 0$ T. The second curve from below was measured at $B = 1$ T. All the other curves correspond to magnetic field induction increments by $\Delta B = 0.5$ T up to $B = 15$ T. The peaks whose evolution is discussed in the present work are marked by small black disks.

In the vicinity of $B = 6$ T, i.e. near an LL filling factor $\nu = 2$, the measured $G(V)$ curves demonstrate (see Fig. 2) a sizable minimum for a zero bias voltage. A further increase in B gradually transforms the minimum into two maxima. A detailed discussion of the tunneling process in the vicinity of zero bias voltage can be found in Ref. [3] and will not be discussed here.

3. Results

Let us discuss the behavior of the 'arms' in the $G(V)$ dependence, which are indicated by small black disks in Fig. 2. The fan-shaped diagram for such transitions is depicted in Fig. 3. Here we consider only negative bias voltages, since the main features of this diagram are symmetric in voltage.

In magnetic fields higher than 12 T and for bias voltages in the vicinity of 30 mV, the small dark disks correspond to a transition between the lower Landau level ($N = 0$) of the ground 2D subband ($n = 0$) in the emitter and the first excited Landau level ($N = 1$) of the ground 2D subband ($n = 0$) in the collector, i.e. $(n = 0, N = 0) \rightarrow (n = 0, N = 1)$. The dashed straight line A has a slope $L\hbar\omega_c$, where ω_c is the cyclotron frequency, and $L = 1.28$ is the electrostatic factor (the ratio of the applied voltage to the voltage falling on the barrier). This

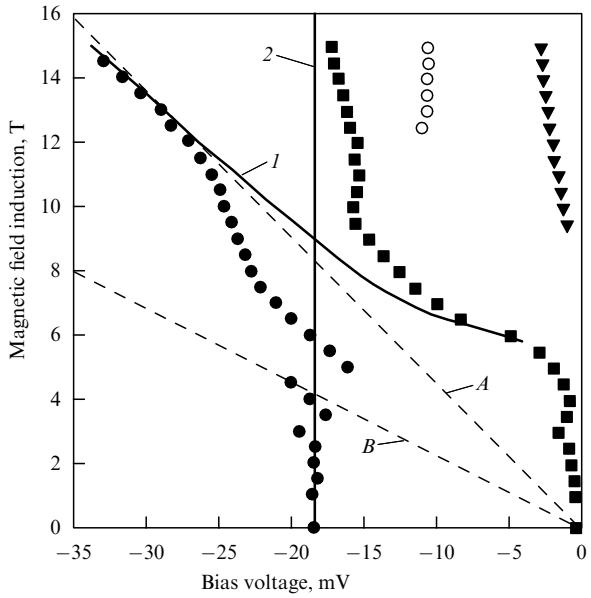

Figure 3. Position of peaks on the bias voltage scale as a function of magnetic field induction. The circles, squares, and triangles represent experimental data and their meaning is discussed in the text. Curve *1* displays the calculated position of the peak in the $(n = 0,\ N = 0) \to (n = 0,\ N = 1)$ transition, where N is the LL number. The vertical line labelled *2* represents the expected position of the peak in the $(n = 0,\ N = 0) \to (n = 1,\ N = 0)$ transition. Neither curve takes into account the interaction between the Landau levels. The straight lines *A* and *B* have slopes $L\hbar\omega_c$ and $2L\hbar\omega_c$, respectively, and describe tunneling between Landau levels with $\Delta N = 1$ and $\Delta N = 2$, where $L = 1.28$.

line demonstrates the position of the peak for tunneling with $\Delta N = 1$ in an approximation that ignores the broadening of the Landau level. The dashed straight line *B* represents (in the same approximation) the position of peaks for tunneling with $\Delta N = 2$.

For broadened Landau levels, the measured differential tunneling conductivity is determined by the density of states at the Fermi level in the emitter 2D system. The calculated positions of the peaks for transitions $(n = 0,\ N = 0) \to (n = 0,\ N = 1)$ between broadened Landau levels is depicted by the solid curve *1*. The position of the peaks corresponding to tunneling with LL number conservation ($\Delta N = 0$) does not depend on the magnetic field intensity and must coincide with the vertical straight line *2*. When there is no interaction between the Landau levels, some of the lines in Fig. 3 should cross, as lines *1* and *2* do. Instead there appears distinct repulsion of the lines consisting of dark disks and squares, which proves the Landau levels $(n = 0,\ N = 1)$ and $(n = 1,\ N = 0)$ interact. The observed splitting is about 10 meV. A certain indication that there is line repulsion can also be seen in the vicinity of the point of crossing of lines *2* and *B*, which corresponds to interaction of the Landau levels $(n = 0,\ N = 2)$ and $(n = 1,\ N = 0)$ in the collector system. Unfortunately, the accuracy of determining the position of the peaks is not high enough to make more specific statements.

To make the picture complete, we also depict the positions of the peaks in the vicinity of zero bias voltage (the triangle-based curves), which have been described by Khanin et al. [3], who studied the tunneling energy gap at the Fermi level in a magnetic field. The origin of the peaks represented by the open circles near 14 mV in magnetic fields higher than 12 T is apparently related to the spin splitting in the system under consideration.

4. Possible reasons for anticrossing

Let us discuss the possible reasons for the strong ($\sim$ 10 meV) anticrossing of the levels $(n = 0,\ N = 1)$ and $(n = 1,\ N = 0)$ observed in our experiments. The mechanism responsible for this effect must mix the longitudinal (along the layer) and transverse (perpendicular to the barrier) electron motions in the quasi-two-dimensional (Q2D) system.

4.1 Misorientation of magnetic field

Experiments in an oblique magnetic field have shown that the precision with which the magnetic field was oriented along the current ($\mathbf{B} \parallel \mathbf{J}$) was sufficiently high to exclude the effect of the magnetic field's component in the sample plane on anticrossing. More exactly, a misorientation ($\mathbf{B}$ and $\mathbf{J}$) of about 5° had no noticeable effect on the pattern in Fig. 3, and there were no noticeable quantitative changes either.

4.2 Nonparabolicity of the electronic spectrum $E(k)$

Another possible reason for anticrossing could be the nonparabolicity of the electronic spectrum $E(k)$ in GaAs. Qualitatively similar anticrossing has been observed in the highly nonparabolic material PbTe [2]. However, in the case of PbTe the strong anticrossing of Landau levels is caused by the fact that the principal axes of the constant-energy ellipsoids of the bottom of the conduction band (the L-points of the Brillouin zone) do not coincide with the direction of growth. This is not true of GaAs, and estimates of the contribution of this effect (nonparabolicity) to anticrossing yield a value of order 1 meV, which is too small to explain the detected effect.

4.3 Tunneling with participation of magnetoplasmons

An alternative explanation of anticrossing is based on collective excitations of the electronic system. Let us discuss the possible mechanisms of energy relaxation of an electron that has tunnelled onto an excited level in a system with a totally discrete spectrum. It is a common fact that if the distance to a low-lying level is an integral multiple of the LO-phonon energy, then the energy relaxation occurs due to resonance emission of such phonons. This corresponds to the appearance of phonon replicas in the tunneling spectrum. In our case such processes are still forbidden (phonon replicas are observed at much higher bias voltages V_b). On the other hand, relaxation accompanied by emission of Q2D magneto-plasmons with a characteristic energy equal either to $\hbar\omega_c$ (intrasubband plasmons) or the distance between the 2D subbands (intersubband plasmons [4]) is allowed in energy. Generally speaking, tunneling processes accompanied by resonance emission of intra- and intersubband 2D magneto-plasmons must manifest themselves in experiments in a way similar to single-particle processes in which the quantum numbers n and N change. The situation is quite different in the vicinity of the point of crossing of the single-particle terms *1* and *2* in Fig. 3. One should expect the Coulomb interaction, which is responsible for the emergence of plasma excitations, to lead to a strong interaction of the two magnetoplasmon branches mentioned earlier precisely in the vicinity of the point where the single-particle terms cross. This fact could be used to explain the observed anticrossing of 'single-particle' terms.

Now we turn to a quantitative description of the spectrum of Q2D magnetoplasmons. There exist a large number of theoretical studies devoted to the plasmon spectrum in Q2D systems. In most of these the plasmons were investigated in the absence of a magnetic field (e.g. see Refs [4–6]). The researchers found that there are two plasmon branches: intrasubband plasmons related to electron oscillations in the ground 2D subband, and intersubband plasmons related to virtual transitions between 2D subbands. The first have a gapless spectrum, while the second exhibit a weak dispersion and a gap with a width equal to the sum of the intersubband energy Δ and the depolarization energy. The interaction of intersubband and intrasubband modes in the absence of a magnetic field is extremely weak even for a specially selected geometry of the structure [7]. A number of papers have been devoted to calculating the spectrum of Q2D plasmons in a magnetic field (e.g. see Refs [8–11]). The results contain an extremely rich structure of the spectrum of such magnetoplasmons but very strongly depend on the approximations employed and the type of a system. We calculated the magnetoplasmon spectrum in the random phase approximation for the structure studied in our experiment. Since plasmons are excited in the process of 2D $\rightarrow$ 2D tunneling in the symmetric system, only antisymmetric (with respect to the barrier's center) plasmon modes are of interest. The result was obtained in the dipole approximation [small wave vectors $\mathbf{q} = (q_x, q_y)$] for fairly strong magnetic fields, when the filling factor is $\nu < 4$.

Our finding is depicted in Fig. 4, where four magnetoplasmon branches are shown, namely, the intersubband branch *1*, the intrasubband branch *2*, and the combined resonance branches *3* and *4* related to virtual transitions between the states $(n = 0, N = 1)$ and $(n = 1, N = 0)$ as well as $(n = 0, N = 0)$ and $(n = 1, N = 1)$. The depolarization energy in this case is close to 4 meV. At $q = 0$, the magnetoplasmon energies coincide with the energies of single-particle excitations depicted in Fig. 4 by lines consisting of small open circles and crosses. Possibly, it was the anticrossing of the branches *1* and *4* that was discovered in our experiments due to the high density of states on these branches. The observed anticrossing of the two peaks can be interpreted as relaxation on 'hybrid' intra- and intersubband magnetoplasmons. The unusual shape of the anticrossing in Fig. 3 is, possibly, related to the effect of branch *2* in Fig. 4.

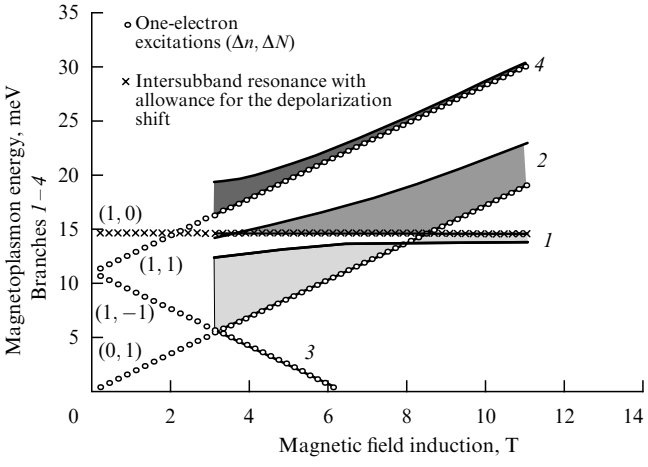

Figure 4. Magnetoplasmon energy (four branches) as a function of magnetic field induction for different wave vectors q. The shaded regions correspond to values of q ranging from zero to 5×10^5 cm^{-1}. Branch *1* represents an intersubband plasmon, branch *2* an intrasubband plasmon, and branches *3* and *4* represent plasmons of a combined resonance with transitions $\Delta - \omega_c$ and $\Delta + \omega_c$, respectively. Lines consisting of small open circles indicate the energy of single-particle excitations $(\Delta n, \Delta N)$; $\Delta = 11$ meV is the intersubband energy.

5. Conclusions

We have studied tunneling between highly disordered 2D electron systems in a quantized magnetic field parallel to the current. A strong interaction between the Landau levels belonging to different 2D subbands has been discovered. We proposed an explanation for the observed anticrossing related to the excitation of intra- and intersubband magnetoplasmons in a Q2D system.

This work was made possible by support given by the Russian Foundation for Basic Research (projects 99-02-17592, 01-02-97020, and 01-02-06476), the Physics of Solid Nanostructures Program, the Surface Atomic Structures Program, and the Physics of Quantum and Wave Processes Program.

References

1. Duke C B *Phys. Rev.* **159** 632 (1967); Ben Daniel D J, Duke C B *Phys. Rev.* **160** 679 (1967); Duke C B *Phys. Lett. A* **24** 461 (1967); Baraff G A, Appelbaum J A *Phys. Rev. B* **5** 475 (1972)
2. Tsui D C, Kaminsky G, Schmidt P H *Phys. Rev. B* **9** 3524 (1974)
3. Khanin Yu N et al. *Physica E* **6** 602 (2000)
4. Dahl D A, Sham L J *Phys. Rev. B* **16** 651 (1977)
5. Vitlina R Z, Chaplik A V *Zh. Eksp. Teor. Fiz.* **81** 1011 (1981) [*Sov. Phys. JETP* **54** 536 (1981)]
6. Jain J K, Das Sarma S *Phys. Rev. B* **36** 5949 (1987)
7. Hu C-M, Schüller C, Heitmann D *Phys. Rev. B* **64** 073303 (2001)
8. Chiu K W, Quinn J J *Phys. Rev. B* **9** 4724 (1974)
9. Tselis A, Quinn J J *Surf. Sci.* **113** 362 (1982)
10. Wendler L, Pechstedt R *J. Phys.: Condens. Matter* **2** 8881 (1990)
11. Bisti V E *Pis'ma Zh. Eksp. Teor. Fiz.* **69** 543 (1999) [*JETP Lett.* **69** 584 (1999)]

PACS numbers: **73.61.–r**, 85.30.Vw, 85.30.Tv

DOI: 10.1070/PU2001v044n12ABEH001057

Quantum dot Ge/Si heterostructures

A V Dvurechenskiĭ, A I Yakimov

1. Introduction

Determining the parameters of the energy spectrum, the kinetics of the transitions between electronic states, and the interaction of elementary excitations and establishing the correlation effects constitute the basis for current fundamental research in the field of quantum dots (QD). Among the numerous heterostructures with quantum dots (see Refs [1–4]) that are being actively studied the silicon-based structures have always provoked special interest, due to the promising integration of the results of such research and the basic silicon technology used in building modern semiconductor devices and circuits. The substantial advances in the epitaxy of Ge on Si and the prospects for using Ge/Si heterostructures formed the natural basis for systems with quantum dots. From the viewpoint of fundamental research,